

Dysregulated wild-type cell division at the interface between host and oncogenic epithelium

Megan Moruzzi¹, Alexander Nestor-Bergmann^{1,2,3}, Keith Brennan⁴, Sarah Woolner^{1,*}

Affiliations:

1: Wellcome Trust Centre for Cell-Matrix Research, Division of Cell Matrix Biology and Regenerative Medicine, School of Biological Sciences, Faculty of Biology, Medicine & Health, Manchester Academic Health Science Centre, University of Manchester, Oxford Road, Manchester M13 9PT, UK

2: School of Mathematics, University of Manchester, Manchester M13 9PL, UK

3: Current address: Department of Physiology, Development and Neuroscience, University of Cambridge, Cambridge, CB2 3DY

4: Division of Cancer Sciences, School of Medical Sciences, Faculty of Biology, Medicine and Health, University of Manchester, Manchester Academic Health Science Centre, Manchester, M13 9PL, UK

Corresponding author: sarah.woolner@manchester.ac.uk

Abstract

Carcinomas dysregulate their microenvironment and this helps aid disease progression, in part by altering the behaviour of host cells from different lineages, such as immune and endothelial cells. However, it remains largely unknown whether small groups of cells with initial oncogenic changes alter their environment or affect fundamental processes, such as cell division, in host epithelia. In this study, clusters of oncogene-expressing cells were created within otherwise normal, *in vivo* tissue, using *Xenopus* embryos. We find that clusters overexpressing $kRas^{V12}$ or cMYC significantly increase cell division in neighbouring host epithelium. Furthermore, we show that hyper-contractility of $kRas^{V12}$ clusters generates forces that deform host epithelia, increasing cell division and biasing division orientation. Contrastingly, cMYC clusters do not induce deformation of surrounding tissue but drive host cell division via a distinct mechanism. Our results indicate novel roles for $kRas^{V12}$ and cMYC, dysregulating cell division in surrounding host, as well as oncogene-expressing, epithelium.

INTRODUCTION

Carcinoma is initiated when a single epithelial cell accumulates genetic changes, which confer the ability to increase cell number [1-6]. *kRas* and *cMYC* are two oncogenes commonly found to be constitutively activated or overexpressed in tumours [7, 8]. Both oncogenes are known to drive cell cycle progression in a cell-autonomous manner, so are thought to give rise to hyperplastic lesions through the clonal expansion of the cell in which they are genetically altered [1, 9, 10]. At later disease stages, *in situ* carcinomas are recognised to alter their microenvironment and contribute to disease progression by dysregulating the behaviour of host cells in different tissue layers [5, 6, 11-24]. However, the local microenvironment could be dysregulated much earlier in the disease process, since the acquisition of a single oncogenic change is sufficient to alter a cell's secretome [15-17, 25-29]. Furthermore, initial driver mutations are likely to perturb the local mechanical environment as, by definition, cell number is increased and, in some cases, normal cytoskeletal dynamics are also disrupted [13, 30-32]. Cell division is sensitive to both chemical and mechanical regulation [33-38], yet whether the acquisition of initial oncogenic changes could alter the microenvironment in a manner that confers upon host cells the ability to increase cell number, rather than solely inducing division in a cell-autonomous manner, has not been studied.

In the early stages of carcinoma, groups of oncogene-expressing cells exist in an otherwise normal, largely intact, epithelial tissue [9, 10]. A handful of studies have demonstrated that the host epithelium recognises the presence of cells with a single oncogenic change and alters its behaviour in response to them. In *Zebrafish*, wild-type epithelial cells that neighbour oncogenic Ras cells suffer ROS stress and release H₂O₂ to attract leukocytes to the site of transformation [39]. Furthermore, in cultured MDCK monolayers, wild-type cells that border individual Ras-expressing cells accumulate the actin cross-linking and stabilising protein, Filamin [40]. Filamin

is required in the surrounding wild-type epithelial cells for Ras cells to be extruded from these epithelial monolayers, indicating that the wild-type neighbours are actively involved in this process [40]. In *Drosophila*, cells that overexpress *dMYC* are not extruded from the epithelium [41], but induce apoptosis in surrounding, wild-type epithelial cells [41-43]. Such changes in the behaviour of host-epithelia have the potential to impact on disease progression, for instance apoptosis of the surrounding wild-type epithelium, as occurs in *Drosophila*, facilitates the expansion of *dMYC* overexpression clones [43]. Conversely increased proliferation could also aid disease progression, as crowding in the epithelia can result in cell delamination, which could expedite the spread of oncogenic cells [44, 45]. However, cell division in the host epithelium, when groups of cells with an initial oncogenic change arise, has not been specifically studied in a vertebrate model.

In this study, we have used *Xenopus laevis* embryos to model an early disease stage and examine the effects oncogenic driver mutations have on cell division in the surrounding host epithelium. A clonal cluster of cells that overexpresses either *kRas*^{V12} or *cMYC* can be easily generated, through the targeted injection of a single cell with mRNA. Previous work has shown that microinjection of oncogenic mRNAs in this manner causes induced tumour-like structures (ITLS) to form in late stage embryos, which exhibit remarkable similarities to human tumours [46-49]. At early gastrula (stage 10), a multi-layered epithelial tissue adhered to a basal fibronectin extracellular matrix (ECM), known as the animal cap, is found across the animal hemisphere of the embryo [50]. Targeted injection of mRNA results in the development of a small group of oncogene-expressing cells within this otherwise wild-type animal cap tissue. By live imaging this tissue, we have examined how overexpression of either *kRas*^{V12} or *cMYC* affects cell division in surrounding host, as well as oncogene-expressing, epithelial tissue. Our results indicate a novel role for

both of these oncogenes in inducing increased and dysregulated cell division in the host epithelium, which has the potential to contribute to their tumourigenic function.

RESULTS

Modelling early stage carcinoma in *Xenopus laevis*

To produce a cluster of oncogene-expressing cells within wild-type *in vivo* epithelial tissue, GFP-*kRas*^{V12} or GFP-cMYC mRNA was injected into a single cell of a stage 6 (32 cell) *Xenopus laevis* embryo (Figure 1A). By early gastrula stage, a cluster of GFP-expressing cells consistently developed in the superficial layer of the animal cap (Figures 1B-D, Figure S1A-B). The cell division rate (CDR) of the oncogene-expressing cells was analysed using time-lapse microscopy. Expression of GFP-*kRas*^{V12} did not drive a significant increase in CDR, in comparison to control-GFP cells ($p > 0.9999$, Figure 1E). However, the GFP-*kRas*^{V12} construct was confirmed functional, as its expression stimulated an increase in ERK phosphorylation (Figure 1F) and, consistent with previous reports from cultured monolayers [51, 52], the GFP-*kRas*^{V12} cells showed an increased propensity to divide out of the epithelial plane (Figure S1C). As previously described [46], ITLS were observed when embryos with GFP-*kRas*^{V12} clusters were developed to later stages, whereas embryos with control-GFP clusters were morphologically normal (Figure 1G-H). Contrasting to existing studies [53-56], we did not observe apical extrusion of any GFP-*kRas*^{V12} cells over the course of our time-lapses (Figure S1D), however on numerous occasions GFP-*kRas*^{V12} expressing cells were observed being lost basally from the superficial layer (Figure 1I-J). Moreover, imaging of fixed, bisected embryos revealed an increased number of cell layers and cells that had completely delaminated from the tissue (Figure S1E-F).

Overexpression of cMYC significantly increased the CDR of cells expressing the oncogene, in comparison to control-GFP cells ($p = 0.0174$, Figure 1E). As in previous

studies, carried out in different embryonic contexts, overexpression of cMYC did not induce apoptosis alongside this increase in cell division (Figure S1G) [57, 58]. Embryos with GFP-cMYC clusters did not develop ITLS at later stages, however this was likely due to fast turnover of the GFP-cMYC mRNA and protein as almost no GFP-positive cells were retained (Figure S1H) [59, 60].

Wild-type epithelium responds to oncogene-expressing clusters with altered cell division

Cancer is a disease characterised by dysregulated cell division and, in later disease stages, wild-type cells derived from non-epithelial tissue layers are stimulated to divide through microenvironment changes induced by tumours [5, 6, 15-24]. We investigated whether cell division might also be altered in the host epithelium during the earliest stages of cancer onset, using the *Xenopus* model. Time-lapse microscopy of gastrula-stage embryos revealed that up to three cells from either GFP-*kRas*^{V12} or GFP-cMYC cell clusters, wild-type epithelial cells showed a significant increase in CDR, compared with equivalent cells in control-GFP embryos ($p=0.0476$ and $p=0.0003$, Figure 2A). This was not a boundary specific effect, as the CDR of wild-type cells in direct contact with the oncogene-expressing cells was not significantly different to that two to three cells away ($p=0.8068$ and $p=0.8406$, Figure 2B). The induction of division in the wild-type epithelium was a localised effect, with cells more than six cells from either GFP-*kRas*^{V12} or GFP-cMYC clusters not displaying a significant difference in CDR, compared with analogous cells in control-GFP embryos ($p>0.9999$ for both, Figure 2A).

The orientation, as well as the frequency, of cell division is usually tightly controlled within epithelial tissues and is vital for maintaining normal tissue architecture [61]. While the *kRas*^{V12}-expressing cells showed an increased propensity to divide out of

the epithelial plane (Figure S1C), wild-type cells up to three cells from both GFP-*kRas*^{V12} and GFP-cMYC clusters retained their strong bias to divide within the plane of the epithelium, with no examples of wild-type cells dividing out of the epithelial plane observed in any of the time-lapses taken (Data not shown, n=10 GFP-*kRas*^{V12} and 9 GFP-cMYC embryos). However, when CDO was examined within the epithelial plane, wild-type cells close to GFP-*kRas*^{V12} clusters appeared to exhibit a directional bias to their division orientations, showing an increased propensity to divide towards the oncogenic cluster (Figure 2C-D). This did not appear to be the case with wild-type cell divisions close to GFP-cMYC clusters, which appeared uniformly oriented within the epithelial plane (Figure 2E). We quantified this effect by measuring the angle between the separating daughter nuclei at anaphase and the closest cluster edge (Figure S2A). Wild-type cells up to six cells from GFP-*kRas*^{V12} clusters had significantly altered CDO within the epithelial plane, compared with equivalent cells in control-GFP embryos (p=0.0207, Figure 2F-G). Wild-type CDO was not significantly altered in cells surrounding GFP-cMYC clusters (p=0.3713, Figure 2H). Across the population of embryos examined, wild-type cells were significantly more likely to orient their divisions 60-90° relative to the GFP-*kRas*^{V12} cluster, compared with wild-type cells close to GFP-control or GFP-cMYC clusters (p=0.0263, Figure S2B). As with CDR, this was a localised effect and wild-type cells more than six cells from the GFP-*kRas*^{V12} cluster did not display a significant difference in CDO compared with those in control-GFP embryos (p=0.5321, Figure S2C-D).

Given that cell division was altered in host epithelium, as well as in the oncogene-expressing cells, we next investigated whether wild-type cells contribute to the ITLS observed in later stage GFP-*kRas*^{V12} embryos. In order to investigate this, cells that neighboured the GFP-*kRas*^{V12} mRNA injected cell, at the 32-cell stage, were injected with mCherry-H2B mRNA. At early gastrula stage, the embryos were screened and those with a GFP-*kRas*^{V12} cell cluster in their superficial layer that was surrounded by

mCherry-H2B expressing cells, but not expressing mCherry-H2B in the GFP-*kRas*^{V12} cluster itself were selected (Figure S2E). At stage 38, the GFP-*kRas*^{V12} driven ITLS were analysed and cells expressing mCherry-H2B were found localised to the growths, demonstrating that cells derived from the host epithelium, as well cells that expressed GFP-*kRas*^{V12}, contributed to the tumour-like phenotype (Figure S2F).

These results show that the host epithelium displays altered cell division in response to groups of cells that overexpress *kRas*^{V12} or *cMYC*. Wild-type cells near oncogene-expressing clusters divided significantly more, in a manner that did not require direct contact with the cluster. Furthermore, wild-type cells close to *kRas*^{V12} cell clusters showed a directional bias in their division orientations within the epithelial plane and exhibited an increased propensity to divide towards the cluster.

***kRas*^{V12} cell clusters impose a mechanical strain on the wild type epithelium**

The changes in cell division observed in the wild-type epithelium close to GFP-*kRas*^{V12} cell clusters are reminiscent of stretched epithelial tissues under anisotropic loading: cells proliferate more and acquire directionality to their divisions, aligning their divisions along the principal axis of cell-level stress [33-36]. In both *Xenopus* and other systems, cell shape has been used to infer mechanical stress in epithelial tissue [35, 62]. Indeed, a popular vertex-based model predicts that, for a cell with mechanically homogenous and isotropic material properties, the principal axis of cell shape, as defined by the position of its tricellular junctions (hereto referred to as the long-axis), aligns exactly with the major axis of cell-level tensile stress [35, 62-65]. We therefore analysed the shape of wild-type cells, to gain insight into mechanical changes across the tissue. Our inferences assume that the cells do not develop anisotropic material properties over time, for example leading to a preferred elongation and orientation.

Up to three cells from GFP-*kRas*^{V12} clusters, wild-type cells were significantly more likely to orient their long-axes in the direction of the cluster, compared with equivalent cells in control-GFP embryos ($p=0.0278$, Figure 3A-B). Wild-type cells up to three cells from GFP-*cMYC* clusters on the other hand, did not show a significant difference in the orientation of their long-axes ($p=0.4424$, Figure 3C). Additionally, cells oriented towards GFP-*kRas*^{V12} clusters were significantly more elongated than corresponding cells in control-GFP embryos ($p=0.0460$, Figure 3D) ($p=0.0460$, Figure 3D). As with the changes in cell division, this change in wild-type tissue geometry was a localised effect: more than three cells from GFP-*kRas*^{V12} cluster, the orientation of cells' long-axes was not significantly different to equivalent cells in control-GFP embryos ($p=0.0956$ and $p=0.9541$ for 4-6 cells and 7 or more cells respectively, Figure S3A-D). Together, these data suggest that cells close to GFP-*kRas*^{V12} clusters are experiencing increased tensile stress in the cluster's direction, whilst cells close to *cMYC* clusters are not.

Mechanical stimuli, including stretch, can induce nuclear localisation of the transcription factor, YAP [33, 66, 67]. Once in the nucleus, YAP binds to one of four TEA domain (TEAD) family transcription factors to regulate target gene expression, resulting in cell cycle progression [33, 66, 68-70]. A dominant negative mCherry-TEAD2 construct (mCherry-TEAD2DN), which sequesters active YAP, was expressed to investigate whether the increase in CDR close to GFP-*kRas*^{V12} clusters was dependent on YAP activity [71]. Interestingly, mCherry-TEAD2DN appeared more nuclear in both the *kRas*-expressing cells and in surrounding wild-type cells (Figure 3E); suggestive of activated YAP signalling. When mCherry-TEAD2DN was expressed in a mosaic manner, specifically in the wild-type epithelium surrounding the GFP-*kRas*^{V12} clusters, the CDR of the mCherry-TEAD2DN cells up to three cells from the cluster, was significantly reduced, compared to wild-type epithelial cells in the same embryos ($p=0.0391$, Figure 3F-G). Expression of mCherry-TEAD2DN did

not significantly alter CDR further from the GFP-*kRas*^{V12} cluster ($p > 0.9999$, Figure 3F-G). This indicates that YAP activity is not usually required to drive cell division in the animal cap at early gastrula stage, however is required to increase the CDR above basal level in cells close to the GFP-*kRas*^{V12} cluster.

Together, these results demonstrate that wild-type cells close to GFP-*kRas*^{V12} cell clusters experience increased tensile strain in the cluster's direction, within the epithelial plane. It is in these same cells that cell division rate and orientation are affected, suggesting a possible association between altered tissue mechanics and altered cell division. Consistent with this hypothesis, our data show that the activity of the known mechanosensitive protein, YAP, is required to drive the increase in CDR in wild-type cells close to GFP-*kRas*^{V12} clusters.

Activation of RhoA in a cell cluster induces a response in the wild-type epithelium comparable to *kRas*^{V12} expression

Stress anisotropy can be generated in epithelial tissues when neighbouring tissues with higher levels of actomyosin contractility exert pulling forces upon them [34, 72-75]. Previous reports have shown that expression of oncogenic Ras stimulates non-transformed mammary epithelial cells to exert increased traction forces on their substrate, in a manner dependent on the activity of Rho and non-muscle myosin II [32]. Myosin II generates contractile forces by crosslinking actin filaments into higher-order structures and hydrolysing ATP to pull on the fibres [76-80] and Ras-expressing cells exhibit increased phosphorylation of myosin II in numerous contexts [32, 53, 81]. Fittingly, in our *Xenopus* model, immunofluorescent staining revealed increased phosphorylated myosin II at tricellular vertices in the *kRas*^{V12}-expressing cells, compared with wild-type cells in these same embryos (Figure 4A). Furthermore, in the *kRas*^{V12} clusters, F-actin organisation was less homogenous, with an increase in cortical actin close to tricellular vertices (Figure 4B). Importantly,

this actin stain did not reveal evidence of an actin ‘purse string’, nor the formation of lamellipodia and filopodia in the wild-type epithelium close to the *kRas*^{V12} cell cluster, making it unlikely that the change in wild-type epithelial cell shape occurred as the result of a wound-healing response that involves chemotaxis of the epithelial sheet towards the *kRas*^{V12}-expressing cells [73, 82-84].

Myosin II is phosphorylated downstream of RhoA activation, which occurs in response to constitutive activation of Ras [85-89]. To explore our hypothesis further and examine whether activation of RhoA is sufficient to induce anisotropic strain in surrounding wild-type tissue, a group of cells were generated that overexpressed the constitutively active RhoA Q63L mutant [90, 91]. Wild-type cells up to three cells from GFP-RhoA^{Q63L} clusters were more likely to orient their long-axes in the cluster’s direction, compared with analogous cells in control-GFP embryos (p=0.0468, Figure 4C-D). Furthermore, the CDO of wild-type cells up to six cells from GFP-RhoA^{Q63L} clusters was significantly different to that observed in control-GFP embryos, with cells showing an increased propensity to orient their divisions towards the cluster, within the epithelial plane (p=0.0368, Figure 4E-F). CDR was also significantly increased in wild-type cells up three cells from GFP-RhoA^{Q63L} clusters, (p=0.0104, Figure 4G). These results demonstrate that a group of cells with increased RhoA activity is sufficient to induce cell shape changes in the surrounding wild-type epithelium, indicative of cell-level anisotropic stresses. Furthermore, the presence of a group of cells with increased RhoA activity can alter wild-type cell division in a similar manner to a *kRas*^{V12} cluster – increasing the CDR and inducing directional bias to division orientations within the epithelial plane.

Non-muscle myosin II is required in *kRas*^{V12}-expressing cells for the cluster to alter wild-type tissue mechanics and cell division

Non-muscle myosin II is required for epithelial cells to generate contractile forces [76-

80]. To directly test whether $kRas^{V12}$ cell contractility is required for the cluster to induce anisotropic cell-level stresses in the surrounding wild-type epithelium, myosin II was knocked down specifically in the $kRas^{V12}$ -expressing cells, through injection of a morpholino (MO) in these cells only [76]. The presence of butterfly-shaped nuclei in the GFP- $kRas^{V12}$ clusters indicated that myosin II levels were reduced, with cells struggling to complete cytokinesis due to the decreased functionality of the actomyosin contractile ring (Figure 5A). The myosin II knockdown did not significantly affect the cell-autonomous CDR of GFP- $kRas^{V12}$ cells ($p=0.4508$, Figure S4A), despite the length of mitosis being significantly longer ($p<0.0001$, Figure S4B). Myosin II knockdown in the GFP- $kRas^{V12}$ clusters did not alter the proportion of cells that divided out of the epithelial plane ($p=0.9571$, Data not shown, $n=5$ control MO GFP- $kRas^{V12}$ and 7 Myosin MO GFP- $kRas^{V12}$ embryos), but did inhibit basal loss of GFP- $kRas^{V12}$ cells from the superficial layer, with no examples observed in any of the time-lapses taken (Data not shown, $n=7$ embryos). When myosin II was knocked-down in the GFP- $kRas^{V12}$ cells, wild-type cells up to three cells from these myosin II-deficient GFP- $kRas^{V12}$ clusters oriented their long-axes uniformly in all directions, on average, within the epithelial plane. The distribution of orientations of these cells' long-axes, relative to the cluster, was no longer significantly different to equivalent cells in control embryos ($p=0.7992$, Figure 5B-C). Therefore, depletion of myosin II in the GFP- $kRas^{V12}$ cells recovered cell shape in the surrounding wild-type epithelium, indicating that isotropic tissue tension had also been restored. Knockdown of myosin II in control-GFP or GFP-cMYC clusters appeared to have no effect on cell shape: surrounding wild-type cells still oriented their long-axes uniformly within the epithelial plane (Figure S4C-D).

Given that surrounding wild-type cell geometry was rescued, we then investigated whether cell division was also recovered. When myosin II was knocked down in the GFP- $kRas^{V12}$ cells, wild-type cells up to six cells from these clusters oriented their

divisions uniformly in all directions within the epithelial plane and CDO was no longer significantly different to analogous cells in control embryos ($p=0.4013$, Figure 5D-E). Myosin II knockdown had no effect on wild-type CDO in control-GFP or GFP-cMYC clusters, with cell divisions being uniformly oriented in all directions within the epithelial plane (Figure S4E-F). Furthermore, the CDR of wild-type cells close to myosin II-deficient $kRas^{V12}$ clusters was significantly reduced compared to wild-type cells close to control-MO $kRas^{V12}$ clusters ($p=0.0299$, Figure 5F). In contrast, knockdown of myosin II in GFP-cMYC clusters did not significantly affect surrounding wild-type CDR, compared with GFP-cMYC control-MO embryos ($p=0.7908$, Figure 5F). Together these data show that myosin II is required in $kRas^{V12}$ cells in order for a GFP- $kRas^{V12}$ cluster to induce anisotropic strain in the surrounding host epithelium and lead to increased CDR and altered CDO in these wild-type cells.

DISCUSSION

The *Xenopus laevis* animal cap provides an *in vivo* vertebrate model in which the response of the host epithelium to clonally developed groups of oncogene-expressing cells can be characterised. In this study, increased cell division was induced in host epithelial tissue up to three cell boundaries from clusters of cells overexpressing either cMYC or $kRas^{V12}$. Moreover, host cell divisions close to $kRas^{V12}$ cell clusters acquired a directional bias not seen in control tissue.

Previous studies have shown that cell division in epithelia can increase in rate and acquire a directional bias following an externally imposed anisotropic mechanical strain, similar to what we see in host cells neighbouring a $kRas^{V12}$ cluster [34, 36, 92-94]. By analysing the orientation of a cell's long axis, we found that wild-type cells close to GFP- $kRas^{V12}$ cell clusters demonstrated features consistent with the presence of anisotropic stress [95], that were absent in wild-type cells close to cMYC expressing clusters [35, 62-65]. Moreover, we found that the GFP- $kRas^{V12}$ dependent

increase in wild-type cell division was dependent on the activity of the known mechanosensitive protein, YAP [33, 66, 67]. Epithelial cells expressing oncogenic Ras are known to exert increased traction forces on their substrate and display increased activation of non-muscle myosin II [32, 53, 81]. In keeping with this, we found that expression of constitutively active RhoA, which activates myosin-II, recapitulates both the directional bias in cell-level stress, and the associated changes in cell division that we see with *kRas*^{V12}. Furthermore, we showed that myosin II was required in *kRas*^{V12} cells for the cluster to induce the changes in tissue mechanics and cell division observed in the surrounding host tissue. Whilst epithelial cells with increased actomyosin contractility have been previously shown to pull on adjoining epithelia, leading to anisotropic loadings and oriented divisions in these neighbouring tissues during developmental processes [34, 72-75], this has never before been reported in the context of oncogenic cells and the wild-type host.

In addition, we also found that wild-type cell division was significantly increased when close to a cluster of cells that overexpress cMYC, however these cells continued to orient their divisions uniformly within the epithelial plane and showed no significant change in their cell shape. Further to this, knockdown of myosin II in the cMYC overexpressing cells did not recover surrounding wild-type cell division rate, implying a distinct mechanism drives increased wild-type cell division in this context. Previous studies have shown that cMYC-overexpression alters a cell's secretome and inhibits the secretion of anti-mitotic factors [28, 29]. Wild-type RPE cells were shown to exhibit increased intracellular ATP when cultured in conditioned media from cMYC-overexpressing cells [28], which could be an indication of increased proliferation [96]. However, such conditioned media experiments have not been carried out alongside assays that measure cell proliferation directly and whether changes in the secretome of cMYC-overexpressing cells can indeed dysregulate cell division in the wild-type epithelium in a disease model remains unknown. Determining whether our

observation of increased cell division in the host epithelium surrounding cMYC overexpressing cell clusters is due to changes in the proteomic microenvironment is an important area for future investigation.

Our results indicate a novel role for *kRas* and cMYC, in inducing cell division in the host epithelium surrounding small groups of cells that have acquired these oncogenic changes. An exciting avenue for future research is to determine whether the same response observed here in embryonic epithelium, also occurs in differentiated, adult tissues during carcinoma onset. If dysregulation of wild-type cell division does indeed occur in host epithelia surrounding developing oncogenic lesions, this could help to drive the increase in cell number that defines disease progression in these early stages. However, the potential impact of host epithelial cell division on disease progression is complex and likely to be highly context dependent. In *Drosophila*, apoptosis in the wild-type epithelium surrounding dMYC overexpressing cell clones facilitates their expansion [43], implying that increased wild-type cell division could have a tumour-suppressive effect. However, proliferation in the host epithelium could also play a role in disease advancement, for instance by contributing to epithelial crowding and cell delamination, aiding the spread of oncogenic cells independently of epithelial-mesenchymal transition [44, 45]. It is also interesting to consider whether the dysregulation of cell division in the host epithelium could increase the chance of these cells acquiring genetic changes of their own. This would imply that primary tumour development, and even the onset of secondary metastases, could be multifocal, arising from genetic damage in multiple cells. As tumour heterogeneity is central to drug resistance, targeting this co-opting of the host epithelium could help to make therapeutic interventions more effective.

MATERIALS AND METHODS

Constructs:

Human *kRas*V12 and cMYC were used in these experiments (Table 1). *kRas* is 82% conserved at the mRNA level between *Xenopus* and mammals, with the proteins encoded for sharing highly similar structures [97]. cMYC is also highly conserved across vertebrates, including *Xenopus* [98] and human cMYC has previously been demonstrated to rescue phenotypes induced in *Xenopus* when endogenous cMYC function is abrogated [99]. Both constructs are also fusion proteins, N-terminally tagged with GFP (Table 1). *kRas* had been N-terminally tagged in numerous studies, with no apparent consequences on its functionality [100]. cMYC has also been N-terminally tagged with GFP in numerous studies, with one study showing GFP-cMYC can functionally replace endogenous cMYC in mice [101].

TABLE 1: Plasmids List

Plasmid	Sources
pCS2 Cherry-Histone 2B	Woolner Lab Stocks
pCS2 BFP-CAAX	Gift from the Bement Lab [102]
pCS2 N-GFP	Woolner Lab Stocks
pCS2 GFP- <i>kRas</i> ^{V12}	pBabe human <i>kRas</i> ^{V12} was purchased from Addgene #2544 and cloned into pCS2 N-GFP (above). PCR primers were used to add 5' BspE1 site and 3' STOP codon and Xho1 site.
pCS2 GFP-cMYC	MSCV human cMYC-IRES-GFP was purchased from Addgene #8119 and cloned into pCS2 N-GFP (above). PCR primers were used to add 5' BspE1 site and 3' STOP codon and Xho1 site.
pCS2 YAP-mKate2	Human YAP in pCDH was a gift from Brennan Lab. pLNT-UbC-mKate2 was a gift from the White Lab. mKate2 was cloned into pCS2. PCR primers were used to add 5' BamH1 site and to remove the 3' STOP codon and add an Xho1 site. YAP was cloned into the resultant pCS2 mKate2 vector. PCR primers were used to add a 5' EcoR1 site and a 3' STOP codon followed by an Xba1 site.
pCS2 TEAD2DN-mCherry	Human TEAD2 Dominant Negative in pCDH was a gift from Brennan Lab and was cloned into pCS2 N-mCherry plasmid (Woolner Lab Stocks). PCR primers were used to add 5' EcoR1 site and to add a 3' STOP codon and followed by an Xba1 site.
pcDNA3-EGFP-RhoA-Q63L	Purchased from Addgene #12968

mRNA Synthesis

Plasmids were linearised by restriction enzyme digestion. The resultant linearised DNA was purified by a phenol/chloroform extraction and *in vitro* capped mRNA

synthesis was carried out according to manufacturer's instructions (*Ambion*, #AM1340). mRNA was then purified by a phenol/chloroform extraction. mRNA was diluted to 1 µg/µl and stored at -80°C until use.

Priming *Xenopus laevis*

Female *Xenopus laevis* were pre-primed with 50 units of Pregnant Mare's Serum Gonadotrophin (Intervet UK) injected into the dorsal lymph sac. Four to seven days later, frogs were then primed with 500 units of Human Chorionic Gonadotrophin (Intervet UK) injected into the dorsal lymph sac [103]. Each frog was housed individually overnight and approximately 18 hrs later, the *Xenopus laevis* were transferred into room temperature (RT) 'high salt' 1x Marc's Modified Ringers (MMR) solution (100 mM NaCl, 2 mM KCl, 1 mM MgCl, and 5 mM HEPES [pH 7.4]). Eggs were collected from tanks 2-5 hours later.

Embryo Fertilisation

In vitro fertilisation was performed as described previously [103]. MMR was removed from the collected eggs. A small amount of testis prep was cut up and spread over collected eggs to ensure all were exposed. After 5 mins at RT, the dish was topped up with 0.1X MMR and left for a further 30 mins. MMR was then drained and the embryos transferred into a glass beaker. 50 ml of 2% L-cysteine solution (2 g L-cysteine (*Sigma Aldrich*, #168149-100G) in 100 ml 0.1% MMR, pH 7.8 - 8.0) was added, and swirled gently until the jelly coat of the embryos was reduced. The L-cysteine solution was then removed and the embryos washed a minimum of six times, with a total 200 ml 0.1% MMR. The embryos were transferred into new 10 ml petri dish and topped up with fresh 0.1% MMR then incubated at RT to reach 2-cell stage.

mRNA Microinjection

Microinjections were carried out using Picospritzer III Intracel injector (Parker instrumentation). Healthy embryos at the 2-cell stage were transferred into an injection dish containing 0.1X MMR with 5% Ficoll (*SigmaAldrich*, #PM400). Each cell was injected with a total volume of 4.2 nl (for constructs and concentrations injected, see Table 2 below). Following this microinjection, embryos were washed in a Petri dish containing 0.1% MMR, then transferred into a second Petri dish containing fresh 0.1% MMR. These embryos were left at RT to develop to the 32-cell stage. At the 32-cell stage, the embryos were transferred back into the injection dish,

containing 0.1% MMR and 0.5% Ficoll, and cells at the animal pole were injected with a total volume of 2.1 nl (for constructs and concentrations injected, see Table 2 below). Following microinjection, the embryos were washed in a Petri dish containing 0.1% MMR and then transferred into a second Petri dish containing fresh 0.1% MMR and incubated at 16°C overnight.

TABLE 2: List of mRNA concentrations injected into *Xenopus* embryos

mRNA Construct	Stage Injected	Total mRNA injected into each cell
Cherry-Histone-H2B	2-cell (both cells)	0.42 ng
Cherry-Histone-H2B	32-cell (multiple cells)	0.21 ng
BFP-CAAX	2-cell (both cells)	0.42 ng
GFP	2-cell (both cells)	0.42 ng
GFP	32-cell (one cell)	0.21 ng
GFP- <i>kRas</i> ^{V12}	2-cell (both cells)	0.42 ng
GFP- <i>kRas</i> ^{V12}	32-cell (one cell)	0.263 ng
GFP-cMYC	2-cell (both cells)	0.42 ng
GFP-cMYC	32-cell (one cell)	0.21 ng
GFP-RhoA ^{Q63L}	32-cell (one cell)	0.105 ng
YAP-mKate2	2-cell (both cells)	0.42 ng
YAP-mKate2	32-cell (multiple cells)	0.21 ng
TEAD2DN-mCherry	32-cell (multiple cells)	0.21 ng

Myosin II Knockdown

Myosin II was knocked down through microinjection of a Morpholino targeting non-muscle myosin II heavy chain 2B (MHC) (Table 3) [76]. Prior to microinjection, the Morpholino was heated for 10 minutes at 65°C and combined with GFP-*kRas*^{V12} mRNA. The final needle concentration of the morpholino was 0.2 µM. A single cell at the animal pole was injected with a total volume of 2.1 nl of the GFP-Ras^{V12} mRNA (above) and MHC Morpholino.

TABLE 3: List of morpholinos injected into *Xenopus* embryos

Morpholino Construct	Morpholino Sequence	Stage when Injected
Control Morpholino	CCTCTTACCTCAG TTACAATTTATA	32-cell (same cell as mRNA microinjection)
Non-Muscle Myosin Heavy Chain 2B	CTTCCTGCCCTGG TCTCTGTGACAT	32-cell (same cell as mRNA microinjection)

Embryo Survival and Cluster Quantification

Following microinjection, embryos were left at 16°C for 16 hrs. At stage 10 [104],

embryos were screened for survival and for the presence of an apical GFP cluster.

Western Blotting

Injected embryos were washed three times in PBS and then lysed by pipetting up and down in 10 μ l ice-cold lysis buffer (Tris-HCl pH7.5, 150 mM NaCl, 0.5% NP-40, 5 mM EGTA, 5 mM EDTA) supplemented with 1X Protease inhibitor cocktail (*Promega G6521*) and PhosSTOP phosphatase inhibitor (*Sigma Aldrich*) per embryo. The embryos were then spun at 16873 x g for ten mins at 4°C and the supernatant transferred into fresh tubes. Up to 10 μ l of each sample was diluted with lysis buffer to make total volume of 15 μ l. 5 μ l of 4X loading buffer (8% SDS, 0.2 M tris-Cl pH 6.8, 8% Glycerol and 0.8% 2-mercaptoethanol) was added and the samples were incubated at 95°C for five mins. Samples were loaded into 4–20% Mini-PROTEAN TGX Stain-Free Protein Gels (*Bio-Ra*, #4568093) and were fractionated by SDS-PAGE, before transfer to a 0.45 μ m nitrocellulose membrane (*GE Healthcare*, #10600002) using a transfer apparatus according to the manufacturer's protocols (*Bio-Rad*). The membrane was blocked by incubation with 5% non-fat milk (or 5% BSA for phospho-specific antibodies) in TBST (10 mM Tris, pH 8.0, 150 mM NaCl, 0.5% Tween 20) for 1 hr. Following this, the membrane was washed once with TBST and incubated with primary antibodies at 4°C for 12 hrs (Phospho-ERK1/2 1:500 (*Sigma Aldrich*, #E7028); ERK1/2 1:1000 (*Cell Signaling*, #9102S), α -tubulin (*Sigma Aldrich*, #T9026)). The antibodies were diluted in the same solution that was used for blocking. Membranes were washed three times for 10 mins with TBST and incubated with IRDye conjugated antibodies (Goat anti-Rabbit IRDye800CW 1:5000 (*abcam*, #216773), donkey anti-mouse IRDye680RD 1:5000 (*abcam*, #216778)), diluted in blocking solution. Membranes were then washed three times more and an Odyssey CLX LICOR was used to image the blot.

Immunofluorescence

Embryos at stage 10 were fixed overnight with a gentle rotation at RT in 'microtubule fix', consisting of 3.7% fresh formaldehyde, 0.25% glutaraldehyde, 0.2% Triton X-100, 69.6 mM K-Pipes, 4.35 mM EGTA, 0.87 mM MgCl₂. The following day, embryos were washed five times with PBS and the vitelline membranes were removed using forceps. Embryos were then quenched in 100 mM sodium borohydride in PBS for 2 hrs, rotating at RT. Embryos were washed three times in PBS for five mins and bleached for 90 mins in 10% H₂O₂ on a lightbox at RT. Embryos were washed three times for ten minutes on a rotator in TBSN (Tris- buffered saline: 155 mM NaCl, 10

mM Tris-Cl [pH 7.4]; 0.1% Nonidet P-40) and then blocked overnight in 10 mg/ml BSA at 4°C with rotation. The block solution was changed twice the following day, and then primary antibodies were added to the embryos at a dilution of 1:200 (GFP-tag (*Invitrogen*, MA5-15256), phospho-myosin light chain 2 (S19) 1:500 (*Cell Signalling*, #3671 lot 3 and lot 6)) and incubated overnight at 4°C. The following day, embryos were washed five times in TBSN/BSA for one hr at 4°C whilst rotating and incubated with secondary antibodies overnight at 4°C at a dilution of 1:400 (Alexa Fluor 488 goat anti-mouse (*Invitrogen*, #A11001) and 1:400 Poly-HRP-conjugated secondary antibody from Tyramide SuperBoost Kits with Alexa Fluor 568 (*ThermoScientific*, #B40956)). Embryos were then washed three times in TBSN/BSA for one hr at 4°C whilst rotating and then twice in TBSN alone for one hour at 4°C. Phospho-myosin light chain 2 was visualised using a Tyramide SuperBoost Kits with Alexa Fluor 568 (*ThermoScientific*, #B40956), according to manufacturers instructions. Nuclei were visualised by staining with DAPI at a dilution of 10 µg/ml (*Thermo-Scientific*, #D1306) and then washed three times in TBSN for half an hour at 4°C.

Phalloidin staining was carried out using albino embryos. Injected embryos were rinsed three times in PBS, and then fixed for four hrs at RT (3.7% formaldehyde, 0.25% glutaraldehyde and 0.1% Triton-X in PBS) whilst rotating gently. Embryos were washed three times in PBS and bisected along the sagittal axis using a razor blade and the vitelline membranes removed using forceps. The embryos were washed a further three times in PBTw (PBS + 0.1% Tween) and incubated overnight whilst rotating at 4°C in 0.005 U/µl Alexa Fluor 594 phalloidin (*Invitrogen*, #A12381) in PBTw. The following day, embryos were washed five times in PBS for one hour whilst rotating at 4°C and imaged.

Live Imaging

Approximately 21 hours after fertilisation, when the embryos were at stage 10 [104], they were transferred into fresh dish of 0.1 X MMR, which had 1 mm Polypropylene mesh (*SpectrumLabs*, P/N146410) stuck to its base to prevent the embryos rolling. Live-imaging was then performed using a dipping lens so as not to apply any mechanical stress by using a coverslip. Images were collected on a Leica TCS SP5 AOBS upright confocal using a 20x/0.50 HCX Apo U-V-I (W (Dipping Lens)) objective and 1x confocal zoom. The confocal settings were as follows: pinhole 1 airy unit, scan speed 1000Hz bi-directional, format 512 x 512. Images were collected using the

following detection mirror settings: BFP 406-483 nm eGFP 498-584 nm and mCherry 604-774 nm using the 405 nm, 488nm (25%) and 594nm (25%) laser lines respectively. Images were collected sequentially to eliminate bleed-through between channels. The distance between each optical stack was maintained at 4.99 μm and the time interval between each capture was 1 min, with each sample imaged for up to 1 hr. The maximum intensity projections of these three-dimensional stacks are shown in the results.

Cell Division Analysis

Embryo time-lapse movies were generated using ImageJ64, from which snapshots were selected. Cell division rate in the epithelial plane was quantified as the percentage of cells where daughter nuclei were observed to separate, per minute. Cells that exhibited nuclear envelope breakdown but where daughter nuclei were not observed to separate within the plane of the epithelium, were assumed to have divided out of plane. In plane CDO was measured using the image J straight-line tool to draw a line between the dividing nuclei of a cell in anaphase and the closest edge of the cluster. Mitotic length was defined as the time between nuclear envelope breakdown and the first frame where daughter nuclei were observed to separate.

Cell Shape Analysis

Cell shape analysis was carried out using software that determines the principle axis of shape by computing eigenvectors of inertia tensor [36, 62].

Analysis of cell shapes was carried out by manually segmenting cells of interest. Cell shape features, such as the principal axis and circularity (described below), were calculated using a previously published in-house Python script [36, 62].

Cell shape was characterised by a shape tensor derived from the second moments of the positions of the tricellular junctions (we also include the rare case where more than three edges meet). For every cell we label the cell vertices $i = 1, 2, \dots, n$ anticlockwise, where n is the number of vertices. The cell centroid, \mathbf{C} , is the arithmetic mean of the positions of the tricellular junctions

$$\mathbf{C} = \frac{1}{n} \sum_{i=1}^n \mathbf{R}_i$$

Where \mathbf{R}_i is the position vector of junction i . The cell shape tensor, S , is then defined as

$$S = \frac{1}{n} \sum_{i=1}^n (\mathbf{R}_i - \mathbf{C}_i) \otimes (\mathbf{R}_i - \mathbf{C}_i)$$

Where \otimes is the outer product. The principal axis of cell shape is defined as the eigenvector associated with the principal eigenvalue of S . Cell circularity is defined as the ratio of the smaller eigenvalue over the larger eigenvalue of S , taking a range between 0 and 1.

Graphs and Statistical analysis

Rose histograms were generated using a python script and all other charts were produced using Prism 7.

Kruskal-Wallis tests were performed on cell division rate data sets to assess statistical significance between multiple unpaired data sets, as normality is not assumed. Mann-Whitney U Tests were performed on cell division rate data sets to assess statistical significance between two data sets, as normality is not assumed. Wilcoxon tests were performed on cell division rate data sets to assess statistical significance between multiple paired data sets, as normality is not assumed. Kolmonov-Smirnov Tests were performed to compare angle data of oncogene and control data sets, as normality is not assumed and this test is sensitive to changes in the angle distributions. Mann-Whitney U Tests were performed to compare elongation scores of oncogene and control data sets, as normality is not assumed and this test is sensitive to changes in median elongation. For all statistical tests performed, n numbers and p values are given in the relevant figure legends.

Acknowledgements

MM was supported by a WT 4 Year PhD Studentship [106506/Z/14/Z], ANB was supported by a BBSRC studentship and SW was supported by a Wellcome Trust/Royal Society Sir Henry Dale Fellowship [098390/Z/12/Z]. The Bioimaging Facility microscopes used in this study were purchased with grants from BBSRC, Wellcome and the University of Manchester Strategic Fund. Thanks to Peter March and Roger Meadows for their help with microscopy and William Bement (University of Wisconsin-Madison) for his kind gift of the BFP-CAAX construct. Also, special thanks to Angeliki Malliri, Paul Martin and Andrew Gilmore for their critical reading of the manuscript.

REFERENCES:

1. Greaves, M. and C.C. Maley, *Clonal evolution in cancer*. Nature, 2012. **481**(7381): p. 306-313.
2. Stratton, M.R., *Exploring the Genomes of Cancer Cells: Progress and Promise*. Science, 2011. **331**(6024): p. 1553-1558.
3. Nowell, P.C., *Clonal evolution of tumor-cell populations*. Science, 1976. **194**(4260): p. 23-28.
4. Miller, S.J., R.M. Lavker, and T.T. Sun, *Interpreting epithelial cancer biology in the context of stem cells: Tumor properties and therapeutic implications*. Biochimica Et Biophysica Acta-Reviews on Cancer, 2005. **1756**(1): p. 25-52.
5. Hanahan, D. and R.A. Weinberg, *The hallmarks of cancer*. Cell, 2000. **100**(1): p. 57-70.
6. Hanahan, D. and R.A. Weinberg, *Hallmarks of Cancer: The Next Generation*. Cell, 2011. **144**(5): p. 646-674.
7. Forbes, S.A., et al., *COSMIC: mining complete cancer genomes in the Catalogue of Somatic Mutations in Cancer*. Nucleic Acids Research, 2011. **39**: p. D945-D950.
8. Kalkat, M., et al., *MYC Deregulation in Primary Human Cancers*. Genes, 2017. **8**(6).
9. Wellings, S.R. and H.M. Jensen, *Origin and progression of ductal carcinoma in human breast*. Journal of the National Cancer Institute, 1973. **50**(5): p. 1111-1118.
10. Allred, D.C., et al., *Ductal carcinoma in situ and the emergence of diversity during breast cancer evolution*. Clinical Cancer Research, 2008. **14**(2): p. 370-378.
11. Bissell, M.J. and W.C. Hines, *Why don't we get more cancer? A proposed role of the microenvironment in restraining cancer progression*. Nature Medicine, 2011. **17**(3): p. 320-329.
12. Khaled, W., et al., *Palpation Imaging using a haptic system for virtual reality applications in medicine*. Medicine Meets Virtual Reality 12: Building a Better You: the Next Tools for Medical Education, Diagnosis , and Care, 2004. **98**: p. 147-153.
13. Butcher, D.T., T. Alliston, and V.M. Weaver, *A tense situation: forcing tumour progression*. Nature Reviews Cancer, 2009. **9**(2): p. 108-122.
14. Cox, T.R. and J.T. Erler, *Remodeling and homeostasis of the extracellular matrix: implications for fibrotic diseases and cancer*. Disease Models & Mechanisms, 2011. **4**(2): p. 165-178.
15. Raghunand, N., R.A. Gatenby, and R.J. Gillies, *Microenvironmental and cellular consequences of altered blood flow in tumours*. British Journal of Radiology, 2003. **76**: p. S11-S22.
16. Tlsty, T.D. and P.W. Hein, *Know thy neighbor: stromal cells can contribute oncogenic signals*. Current Opinion in Genetics & Development, 2001. **11**(1): p. 54-59.
17. Bhowmick, N.A., E.G. Neilson, and H.L. Moses, *Stromal fibroblasts in cancer initiation and progression*. Nature, 2004. **432**(7015): p. 332-337.
18. DeNardo, D., P. Andreu, and L.M. Coussens, *Interactions between lymphocytes and myeloid cells regulate pro- versus anti-tumor immunity*. Cancer and Metastasis Reviews, 2010. **29**(2): p. 309-316.
19. Grivennikov, S.I., F.R. Greten, and M. Karin, *Immunity, Inflammation, and Cancer*. Cell, 2010. **140**(6): p. 883-899.
20. Qian, B.Z. and J.W. Pollard, *Macrophage Diversity Enhances Tumor Progression and Metastasis*. Cell, 2010. **141**(1): p. 39-51.
21. Colotta, F., et al., *Cancer-related inflammation, the seventh hallmark of cancer: links to genetic instability*. Carcinogenesis, 2009. **30**(7): p. 1073-1081.

22. Hanahan, D. and L.M. Coussens, *Accessories to the Crime: Functions of Cells Recruited to the Tumor Microenvironment*. Cancer Cell, 2012. **21**(3): p. 309-322.
23. Calvo, F., et al., *Mechanotransduction and YAP-dependent matrix remodelling is required for the generation and maintenance of cancer-associated fibroblasts*. Nature Cell Biology, 2013. **15**(6): p. 637-+.
24. Zhang, K., et al., *Mechanical signals regulate and activate SNAIL1 protein to control the fibrogenic response of cancer-associated fibroblasts*. Journal of Cell Science, 2016. **129**(10): p. 1989-2002.
25. Edwards, P.A.W., *Heterogenous expression of cell-surface antigens in normal epithelia and their tumors, revealed by monoclonal-antibodies*. British Journal of Cancer, 1985. **51**(2): p. 149-160.
26. Fidler, I.J., *Timeline - The pathogenesis of cancer metastasis: the 'seed and soil' hypothesis revisited*. Nature Reviews Cancer, 2003. **3**(6): p. 453-458.
27. Albini, A. and M.B. Sporn, *The tumour microenvironment as a target for chemoprevention*. Nature Reviews Cancer, 2007. **7**(2): p. 139-147.
28. Pocsfalvi, G., et al., *Analysis of Secretome Changes Uncovers an Autocrine/Paracrine Component in the Modulation of Cell Proliferation and Motility by c-Myc*. Journal of Proteome Research, 2011. **10**(12): p. 5326-5337.
29. Cowling, V.H., et al., *c-Myc transforms human mammary epithelial cells through repression of the Wnt inhibitors DKK1 and SFRP1*. Molecular and Cellular Biology, 2007. **27**(14): p. 5135-5146.
30. Paszek, M.J., et al., *Tensional homeostasis and the malignant phenotype*. Cancer Cell, 2005. **8**(3): p. 241-254.
31. Beil, M., et al., *Sphingosylphosphorylcholine regulates keratin network architecture and visco-elastic properties of human cancer cells*. Nature Cell Biology, 2003. **5**(9): p. 803-811.
32. Zhong, C.L., M.S. Kinch, and K. Burridge, *Rho-stimulated contractility contributes to the fibroblastic phenotype of ras-transformed epithelial cells*. Molecular Biology of the Cell, 1997. **8**(11): p. 2329-2344.
33. Benham-Pyle, B.W., B.L. Pruitt, and W.J. Nelson, *Mechanical strain induces E-cadherin-dependent Yap1 and beta-catenin activation to drive cell cycle entry*. Science, 2015. **348**(6238): p. 1024-1027.
34. Campinho, P., et al., *Tension-oriented cell divisions limit anisotropic tissue tension in epithelial spreading during zebrafish epiboly*. Nature Cell Biology, 2013. **15**(12): p. 1405-+.
35. LeGoff, L., H. Rouault, and T. Lecuit, *A global pattern of mechanical stress polarizes cell divisions and cell shape in the growing Drosophila wing disc*. Development, 2013. **140**(19): p. 4051-4059.
36. Nestor-Bergmann, A., et al., *Decoupling the roles of cell shape and mechanical stress in orienting and cueing epithelial mitosis*. bioRxiv, 2018.
37. Howe, A., et al., *Integrin signaling and cell growth control*. Current Opinion in Cell Biology, 1998. **10**(2): p. 220-231.
38. Alberts, B., et al., *Molecular Biology of the Cell*, ed. G. Science. Vol. 6. 2014.
39. Feng, Y., et al., *Live Imaging of Innate Immune Cell Sensing of Transformed Cells in Zebrafish Larvae: Parallels between Tumor Initiation and Wound Inflammation*. Plos Biology, 2010. **8**(12).
40. Kajita, M., et al., *Interaction with surrounding normal epithelial cells influences signalling pathways and behaviour of Src-transformed cells*. Journal of Cell Science, 2010. **123**(2): p. 171-180.
41. Leung, C.T. and J.S. Brugge, *Outgrowth of single oncogene-expressing cells from suppressive epithelial environments*. Nature, 2012. **482**(7385): p. 410-U160.

42. de la Cova, C., et al., *Drosophila Myc regulates organ size by inducing cell competition*. Cell, 2004. **117**(1): p. 107-116.
43. Moreno, E. and K. Basler, *dMyc transforms cells into super-competitors*. Cell, 2004. **117**(1): p. 117-129.
44. Marinari, E., et al., *Live-cell delamination counterbalances epithelial growth to limit tissue overcrowding*. Nature, 2012. **484**(7395): p. 542-U177.
45. Eisenhoffer, G.T., et al., *Crowding induces live cell extrusion to maintain homeostatic cell numbers in epithelia*. Nature, 2012. **484**(7395): p. 546-U183.
46. Chernet, B.T. and M. Levin, *Transmembrane voltage potential of somatic cells controls oncogene-mediated tumorigenesis at long-range*. Oncotarget, 2014. **5**(10): p. 3287-3306.
47. Dahmane, N., et al., *Activation of the transcription factor Gli1 and the Sonic hedgehog signalling pathway in skin tumours*. Nature, 1997. **389**(6653): p. 876-881.
48. Wallingford, J.B., et al., *p53 activity is essential for normal development in Xenopus*. Current Biology, 1997. **7**(10): p. 747-757.
49. Yang, S.S., et al., *Overexpression of a novel Xenopus Rel mRNA induces tumors in early embryos*. Journal of Biological Chemistry, 1998. **273**(22): p. 13746-13752.
50. Nandadasa, S., et al., *Regulation of Classical Cadherin Membrane Expression and F-Actin Assembly by Alpha-Catenins, during Xenopus Embryogenesis*. Plos One, 2012. **7**(6).
51. Magudia, K., A. Lahoz, and A. Hall, *K-Ras and B-Raf oncogenes inhibit colon epithelial polarity establishment through up-regulation of c-myc*. Journal of Cell Biology, 2012. **198**(2): p. 185-194.
52. Schoenenberger, C.A., et al., *Multilayering and loss of apical polarity in mdck cells transformed with viral k-ras*. Journal of Cell Biology, 1991. **112**(5): p. 873-889.
53. Hogan, C., et al., *Characterization of the interface between normal and transformed epithelial cells*. Nature Cell Biology, 2009. **11**(4): p. 460-U234.
54. Kajita, M., et al., *Filamin acts as a key regulator in epithelial defence against transformed cells*. Nature Communications, 2014. **5**.
55. Kon, S., K. Ishibashi, and Y. Fujita, *Cell competition with normal epithelial cells promotes apical extrusion of transformed cells through metabolic changes*. Cancer Science, 2018. **109**: p. 143-143.
56. Ohoka, A., et al., *EPLIN is a crucial regulator for extrusion of RasV12-transformed cells*. Journal of Cell Science, 2015. **128**(4): p. 781-789.
57. Beer, S., et al., *Developmental context determines latency of MYC-induced tumorigenesis*. Plos Biology, 2004. **2**(11): p. 1785-1798.
58. Claveria, C., et al., *Myc-driven endogenous cell competition in the early mammalian embryo*. Nature, 2013. **500**(7460): p. 39-U53.
59. Dani, C., et al., *Extreme instability of myc messenger-RNA in normal and transformed human-cells*. Proceedings of the National Academy of Sciences of the United States of America-Biological Sciences, 1984. **81**(22): p. 7046-7050.
60. Hann, S.R. and R.N. Eisenman, *Proteins encoded by the human c-myc oncogene - Differential expression in neoplastic-cells*. Molecular and Cellular Biology, 1984. **4**(11): p. 2486-2497.
61. Pease, J.C. and J.S. Tirnauer, *Mitotic spindle misorientation in cancer - out of alignment and into the fire*. Journal of Cell Science, 2011. **124**(7): p. 1007-1016.
62. Nestor-Bergmann, A., et al., *Relating cell shape and mechanical stress in a spatially disordered epithelium using a vertex-based model*. Mathematical Medicine and Biology-a Journal of the Ima, 2018. **35**: p. 1-27.

63. Chiou, K.K., L. Hufnagel, and B.I. Shraiman, *Mechanical Stress Inference for Two Dimensional Cell Arrays*. Plos Computational Biology, 2012. **8**(5).
64. Ishihara, S. and K. Sugimura, *Bayesian inference of force dynamics during morphogenesis*. Journal of Theoretical Biology, 2012. **313**: p. 201-211.
65. Brodland, G.W., et al., *CellFIT: A Cellular Force-Inference Toolkit Using Curvilinear Cell Boundaries*. Plos One, 2014. **9**(6).
66. Aragona, M., et al., *A Mechanical Checkpoint Controls Multicellular Growth through YAP/TAZ Regulation by Actin-Processing Factors*. Cell, 2013. **154**(5): p. 1047-1059.
67. Fletcher, G.C., et al., *The Spectrin cytoskeleton regulates the Hippo signalling pathway*. Embo Journal, 2015. **34**(7): p. 940-954.
68. Aktas, H., H. Cai, and G.M. Cooper, *Ras links growth factor signaling to the cell cycle machinery via regulation of cyclin D1 and the Cdk inhibitor p27(KIP1)*. Molecular and Cellular Biology, 1997. **17**(7): p. 3850-3857.
69. Johnson, R. and G. Halder, *The two faces of Hippo: targeting the Hippo pathway for regenerative medicine and cancer treatment*. Nature Reviews Drug Discovery, 2014. **13**(1): p. 63-79.
70. Low, B.C., et al., *YAP/TAZ as mechanosensors and mechanotransducers in regulating organ size and tumor growth*. Febs Letters, 2014. **588**(16): p. 2663-2670.
71. Liu-Chittenden, Y., et al., *Genetic and pharmacological disruption of the TEAD-YAP complex suppresses the oncogenic activity of YAP*. Genes & Development, 2012. **26**(12): p. 1300-1305.
72. Aigouy, B., et al., *Cell Flow Reorients the Axis of Planar Polarity in the Wing Epithelium of Drosophila*. Cell, 2010. **142**(5): p. 773-786.
73. Behrndt, M., et al., *Forces Driving Epithelial Spreading in Zebrafish Gastrulation*. Science, 2012. **338**(6104): p. 257-260.
74. Charras, G. and A.S. Yap, *Tensile Forces and Mechanotransduction at Cell-Cell Junctions*. Current Biology, 2018. **28**(8): p. R445-R457.
75. Etournay, R., et al., *Interplay of cell dynamics and epithelial tension during morphogenesis of the Drosophila pupal wing*. Elife, 2015. **4**.
76. Skoglund, P., et al., *Convergence and extension at gastrulation require a myosin IIB-dependent cortical actin network*. Development, 2008. **135**(14): p. 2435-2444.
77. Bhatia-Dey, N., et al., *Differential expression of non-muscle myosin heavy chain genes during Xenopus embryogenesis*. Mechanisms of Development, 1998. **78**(1-2): p. 33-36.
78. Geeves, M.A. and K.C. Holmes, *The molecular mechanism of muscle contraction*. Fibrous Proteins: Muscle and Molecular Motors, 2005. **71**: p. 161-+.
79. Rayment, I. and H.M. Holden, *THE 3-DIMENSIONAL STRUCTURE OF A MOLECULAR MOTOR*. Trends in Biochemical Sciences, 1994. **19**(3): p. 129-134.
80. Conti, M.A. and R.S. Adelstein, *Nonmuscle myosin II moves in new directions*. Journal of Cell Science, 2008. **121**(1): p. 11-18.
81. Bosveld, F., et al., *Modulation of junction tension by tumor suppressors and proto-oncogenes regulates cell-cell contacts*. Development, 2016. **143**(4): p. 623-634.
82. Martin, P. and J. Lewis, *Actin cables and epidermal movement in embryonic wound-healing*. Nature, 1992. **360**(6400): p. 179-183.
83. Omelchenko, T., et al., *Rho-dependent formation of epithelial "leader" cells during wound healing*. Proceedings of the National Academy of Sciences of the United States of America, 2003. **100**(19): p. 10788-10793.

84. Poujade, M., et al., *Collective migration of an epithelial monolayer in response to a model wound*. Proceedings of the National Academy of Sciences of the United States of America, 2007. **104**(41): p. 15988-15993.
85. Chen, J.C., et al., *Oncogenic Ras leads to Rho activation by activating the mitogen-activated protein kinase pathway and decreasing Rho-GTPase-activating protein activity*. Journal of Biological Chemistry, 2003. **278**(5): p. 2807-2818.
86. Sahai, E., M.F. Olson, and C.J. Marshall, *Cross-talk between Ras and Rho signalling pathways in transformation favours proliferation and increased motility*. Embo Journal, 2001. **20**(4): p. 755-766.
87. Zondag, G.C.M., et al., *Oncogenic Ras downregulates Rac activity, which leads to increased Rho activity and epithelial-mesenchymal transition*. Journal of Cell Biology, 2000. **149**(4): p. 775-781.
88. Riento, K. and A.J. Ridley, *Rocks: Multifunctional kinases in cell behaviour*. Nature Reviews Molecular Cell Biology, 2003. **4**(6): p. 446-456.
89. Leung, T., et al., *The p160 RhoA-binding kinase ROK alpha is a member of a kinase family and is involved in the reorganization of the cytoskeleton*. Molecular and Cellular Biology, 1996. **16**(10): p. 5313-5327.
90. Ghosh, P.M., et al., *Role of RhoA activation in the growth and morphology of a murine prostate tumor cell line*. Oncogene, 1999. **18**(28): p. 4120-4130.
91. Longenecker, K., et al., *Structure of a constitutively activated RhoA mutant (Q63L) at 1.55 angstrom resolution*. Acta Crystallographica Section D-Biological Crystallography, 2003. **59**: p. 876-880.
92. Hart, K.C., et al., *E-cadherin and LGN align epithelial cell divisions with tissue tension independently of cell shape*. Proceedings of the National Academy of Sciences of the United States of America, 2017. **114**(29): p. E5845-E5853.
93. Gudipaty, S.A., et al., *Mechanical stretch triggers rapid epithelial cell division through Piezo1*. Nature, 2017. **543**(7643): p. 118-+.
94. Wyatt, T.P.J., et al., *Emergence of homeostatic epithelial packing and stress dissipation through divisions oriented along the long cell axis*. Proceedings of the National Academy of Sciences of the United States of America, 2015. **112**(18): p. 5726-5731.
95. Nestor-Bergmann, A., et al., *Mechanical characterization of disordered and anisotropic cellular monolayers*. Physical Review E, 2018. **97**(5).
96. Crouch, S.P.M., et al., *The use of ATP bioluminescence as a measure of cell-proliferation and cytotoxicity*. Journal of Immunological Methods, 1993. **160**(1): p. 81-88.
97. Baum, E.Z. and G.A. Bebernitz, *K-RAS ONCOGENE EXPRESSION IN XENOPUS-LAEVIS*. Oncogene, 1990. **5**(5): p. 763-767.
98. Taylor, M., et al., *Xenopus myc proto-oncogene during development: expression as a stable maternal mRNA uncoupled from cell division*. European Molecular Biology Organization, 1986. **20;5(13)**(13): p. 3563-70.
99. Etard, C., et al., *Pontin and Reptin regulate cell proliferation in early Xenopus embryos in collaboration with c-Myc and Miz-1*. Mechanisms of Development, 2005. **122**(4): p. 545-556.
100. Michaelson, D. and M. Philips, *The use of GFP to localize Rho GTPases in living cells*, in *Methods in Enzymology, Vol 406, Regulators and Effectors of Small Gtpases: Rho Family*, W.E. Balch, C.J. Der, and A. Hall, Editors. 2006, Elsevier Academic Press Inc: San Diego. p. 296-315.
101. Huang, C.Y., et al., *Dynamic regulation of c-Myc proto-oncogene expression during lymphocyte development revealed by a GFP-c-Myc knock-in mouse*. European Journal of Immunology, 2008. **38**(2): p. 342-349.
102. Larson, M.E. and W.M. Bement, *Automated mitotic spindle tracking suggests a link between spindle dynamics, spindle orientation, and anaphase onset in epithelial cells*. Molecular Biology of the Cell, 2017. **28**(6): p. 746-759.

103. Woolner, S., A.L. Miller, and W.M. Bement, *Imaging the Cytoskeleton in Live Xenopus laevis Embryos*. Cytoskeleton Methods and Protocols, 2009. **586**: p. 23-39.
104. P, N. and F. J., *Normal Table of Xenopus laevis (Daudin)*. 1994, New York: Garland Publishing Inc.

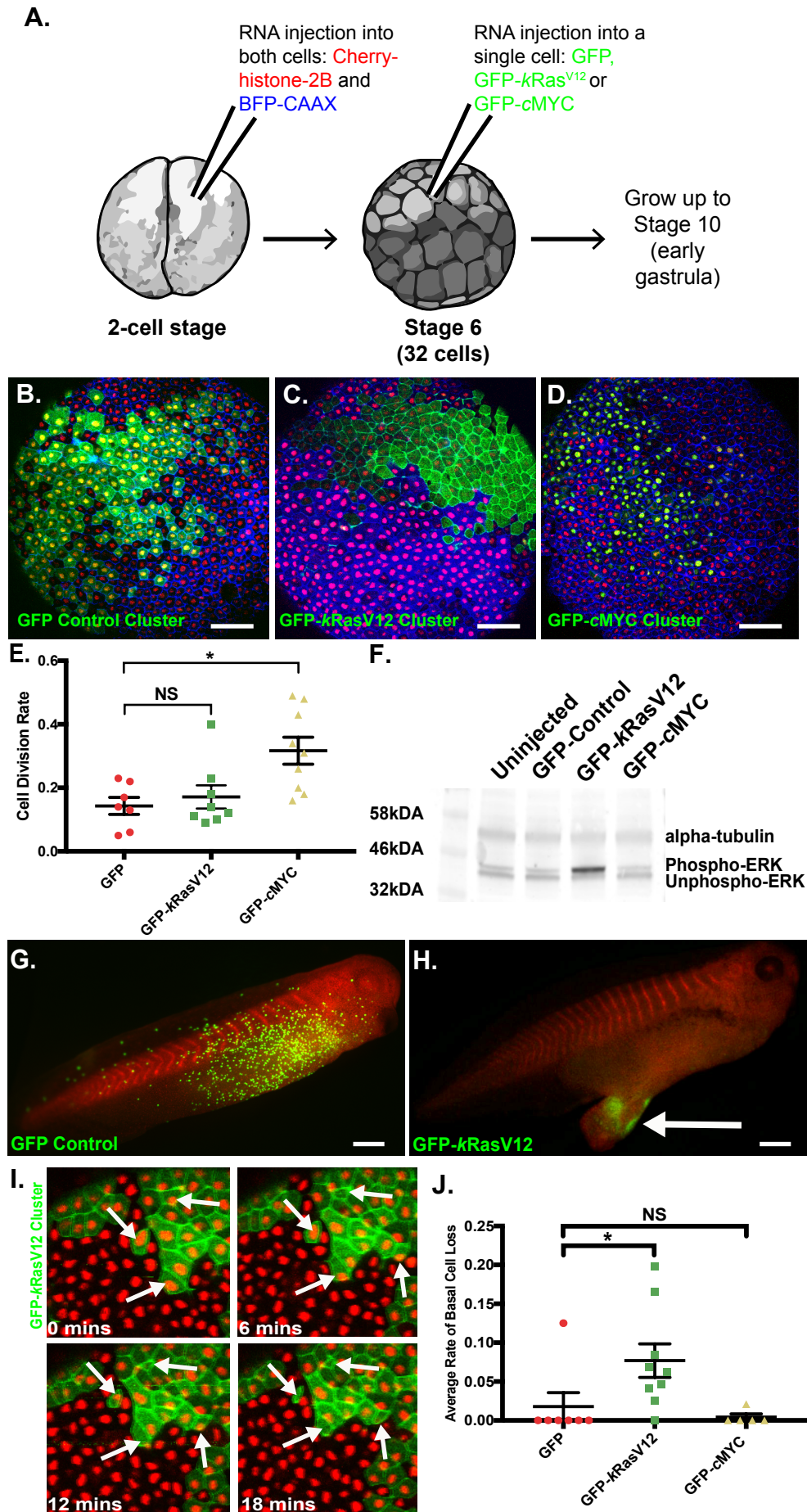


Figure 1: Modelling early stage carcinoma in *Xenopus laevis*

A. Schematic of the microinjection protocol. *Xenopus* embryos were injected with Cherry Histone H2B and BFP-CAAX mRNA at the 2-cell stage. At the 32-cell stage, a single cell was injected with GFP, GFP-*kRas*^{V12} or GFP-cMYC mRNA. Embryos were developed to early gastrula stage 10 and imaged. **B-D.** Confocal microscopy images of *Xenopus* embryos developed to early gastrula stage 10, following injection of a single cell at the 32-cell stage with (B) GFP, (C) GFP-*kRas*^{V12} or (D) GFP-cMYC mRNA. **E.** Scatter Plot shows the average percentage of cells that divided per minute of time-lapse, in either GFP, GFP-*kRas*^{V12} or GFP-cMYC overexpression clusters. Kruskal-Wallis test: $p > 0.9999$ and $p = 0.0174$, $n = 7$ GFP-control, 8 GFP-*kRas*^{V12} and 9 GFP-cMYC embryos. Error bars show SEM. **F.** Western blot shows phosphorylated ERK, unphosphorylated ERK and α -tubulin expression in uninjected control embryos and in embryos injected with GFP, GFP-*kRas*^{V12} or GFP-cMYC mRNA at the 32-cell stage. Embryos were lysed at early gastrula stage 10. **G-H.** Microscopy images show representative embryos at stage 38 that had a (G) GFP or (H) GFP-*kRas*^{V12} expressing cluster at stage 10. Anterior is towards the right. Scale bars are 500 μ m. **I.** Stills from a confocal microscopy time-lapse of a representative embryo with a GFP-*kRas*^{V12} cell cluster at stage 10. White arrows highlight nuclei observed to be lost basally over the course of the time-lapse. **J.** Scatter plot shows average percentage of cells that basally delaminated from GFP, GFP-*kRas*^{V12} or GFP-cMYC cell clusters. Kruskal-Wallis test: $p = 0.0157$ and > 0.9999 , $n = 7$ GFP, 9 GFP-*kRas*^{V12} and 5 GFP-cMYC. Error bars are SEM.

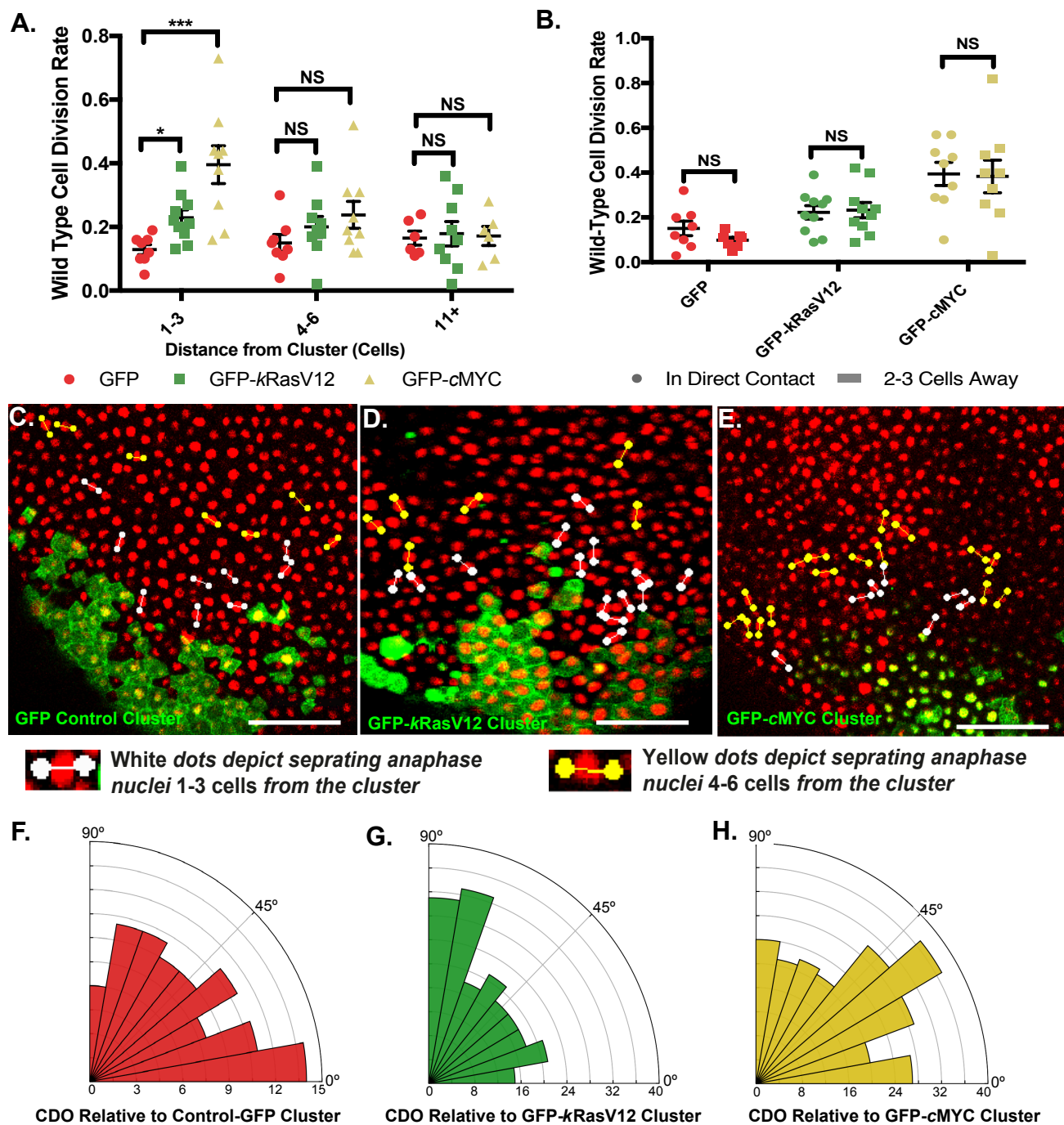


Figure 2: The wild-type epithelium responds to oncogene-expressing clusters with altered

A-B. Scatter Plots show the percentage of wild-type cells that divided per minute of time-lapse at different distances from GFP, GFP-*kRas*^{V12} or GFP-cMYC clusters. (A) 1-3 cells: Kruskal-Wallis test: $p=0.0476$ and 0.0003 , $n=8$ GFP-control, 10 GFP-*kRas*^{V12} and 9 GFP-cMYC embryos. 4-6 cells: $p=0.2654$ and 0.1574 , $n=8$ GFP-control, 9 GFP-*kRas*^{V12} and 9 GFP-cMYC embryos. 7+ cells: $p>0.9999$ for both, $n=6$ GFP-control, 9 GFP-*kRas*^{V12} and 6 GFP-cMYC embryos. Error bars are SEM. (B) GFP: Paired t-test: $p=0.4177$, $n=8$ embryos. GFP-*kRas*^{V12}: $p=0.8068$, $n=10$ embryos, GFP-cMYC: $p=0.8406$, $n=9$ embryos. **C-E.** Snapshots from confocal microscopy time-lapses of representative embryos showing the orientation of cell divisions that occurred in wild-type cells: coloured lines were drawn connecting the dividing anaphase nuclei. White lines label divisions 1-3 cells from the cluster and yellow lines mark divisions 4-6 cells away. Scale bars are 100 μm . **F-H.** Rose histograms show cell division orientation relative to (F) GFP control (G) GFP-*kRas*^{V12} and (H) GFP-cMYC clusters, with the total number of cell divisions analysed across all embryos in each data group in 10° bins. GFP vs. GFP-*kRas*^{V12}: Kolmogorov-Smirnov Test: $p=0.0207$, $n=88$ divisions from GFP embryos and 193 divisions from GFP-*kRas*^{V12} embryos. GFP vs. GFP-cMYC: Kolmogorov-Smirnov Test: $p=0.3713$, $n=88$ divisions from GFP embryos and 231 divisions from GFP-cMYC embryos.

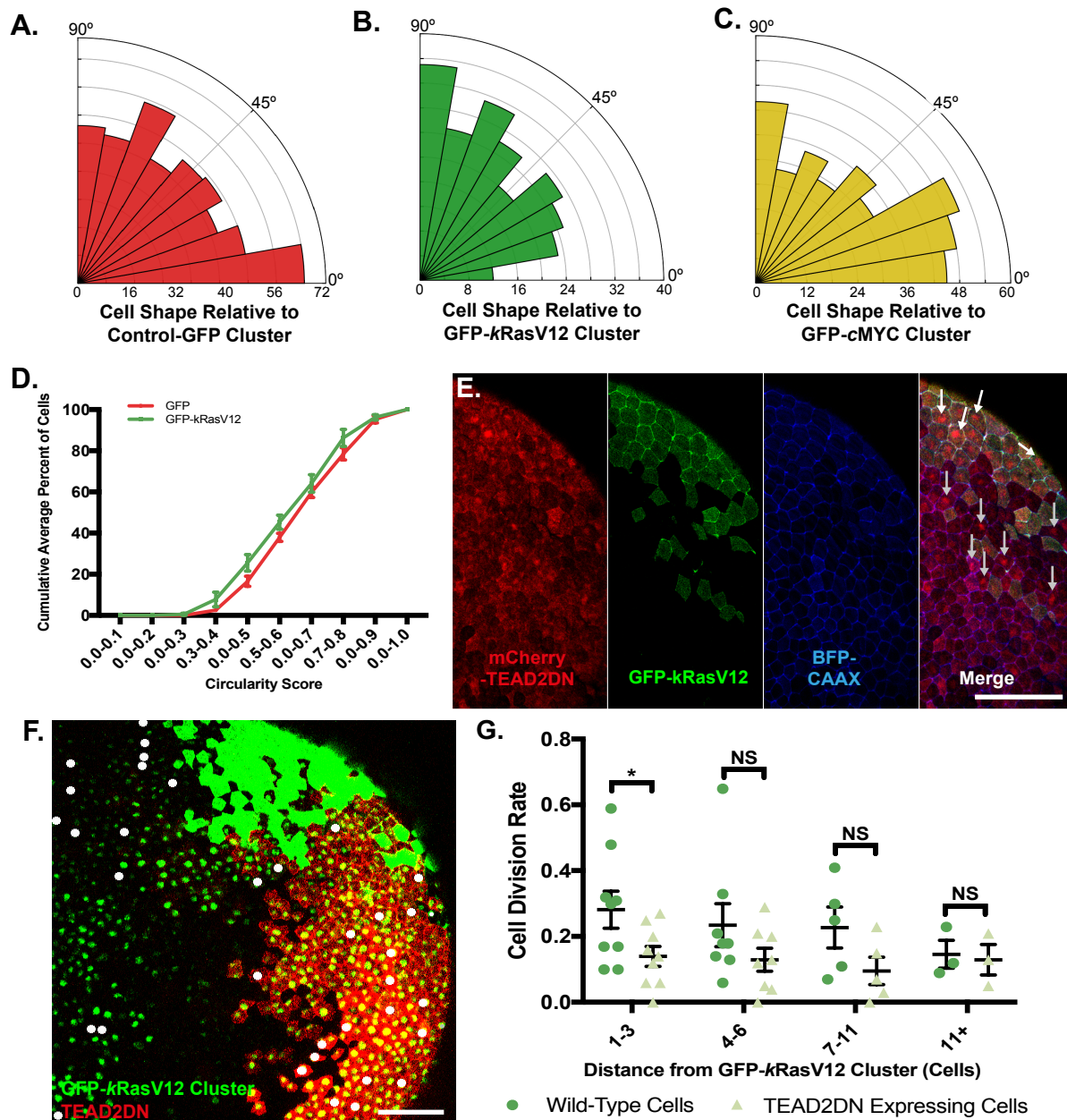


Figure 3: *kRas*^{V12} cell cluster impose a mechanical strain on the wild type epithelium

A-C. Rose histograms show the orientation of wild-type cells' long-axes 1-3 cells from a (A) GFP-control (B) GFP-*kRas*^{V12} and (C) GFP-cMYC clusters, relative to the cluster, with the total number of cells analysed across all embryos in each data group in 10° bins. GFP vs. GFP-*kRas*^{V12}: Kolmogorov-Smirnov Test: $p=0.0278$, $n=346$ divisions from GFP embryos and 224 cells from GFP-*kRas*^{V12} embryos. GFP vs. GFP-cMYC: Kolmogorov-Smirnov Test: $p=0.4424$, $n=333$ cells from GFP embryos and 224 cells from GFP-cMYC embryos. **D.** Analysis of cell elongation was carried out up to 3 cells from control GFP and GFP-*kRas*^{V12} cluster, on cells that were oriented towards the cluster (45°-90). Cell elongation was calculated by dividing the length of a cell's minor axis (the axis perpendicular to its major axis) by the length of its major axis. The line graph shows the average cumulative percentage of cells. Mann-Whitney U Test: $p=0.0460$, 168 cells from GFP embryos and 127 cells from GFP-*kRas*^{V12} embryos. Error bars show SEM. **E.** Confocal microscopy image of a stage 10 *Xenopus* embryo injected with BFP-CAAX (blue) and mCherry-TEAD2DN (red) mRNA at the 2-cell stage and injected with GFP-*kRas*^{V12} (green) mRNA in a single cell at the 32-cell stage. Arrows highlight cells where mCherry-TEAD2DN appears more nuclear. Scale bar is 100 μm . **F.** Confocal microscopy image of a stage 10 *Xenopus* embryo injected with GFP-H2B (green) at the 2-cell stage and injected with GFP-*kRas*^{V12} (green) mRNA in a single cell at the 32-cell stage; mCherry-TEAD2DN (red) mRNA was then injected into two neighbouring cells. Dots highlight cells that underwent division over the course of the time-lapse. Scale bar is 100 μm . **G.** Scatter Plot shows percentage of wild-type or mCherry-TEAD2DN cells that divided per minute of time-lapse at different distances from the GFP-*kRas*^{V12} cluster Error bars show SEM. 1-3 cells: Wilcoxon test 1-3 cells: $p=0.0391$, $n=9$ GFP-*kRas*^{V12} and mCherry-TEAD2DN mosaic embryos. 4-6 cells: $p=0.3281$, $n=8$ GFP-*kRas*^{V12} and mCherry-TEAD2DN mosaic embryos. 7-11 cells: $p=0.1250$, $n=5$ GFP-*kRas*^{V12} and mCherry-TEAD2DN mosaic embryos. 12+ cells: $p>0.9999$, $n=3$ GFP-*kRas*^{V12} and mCherry-TEAD2DN mosaic embryos

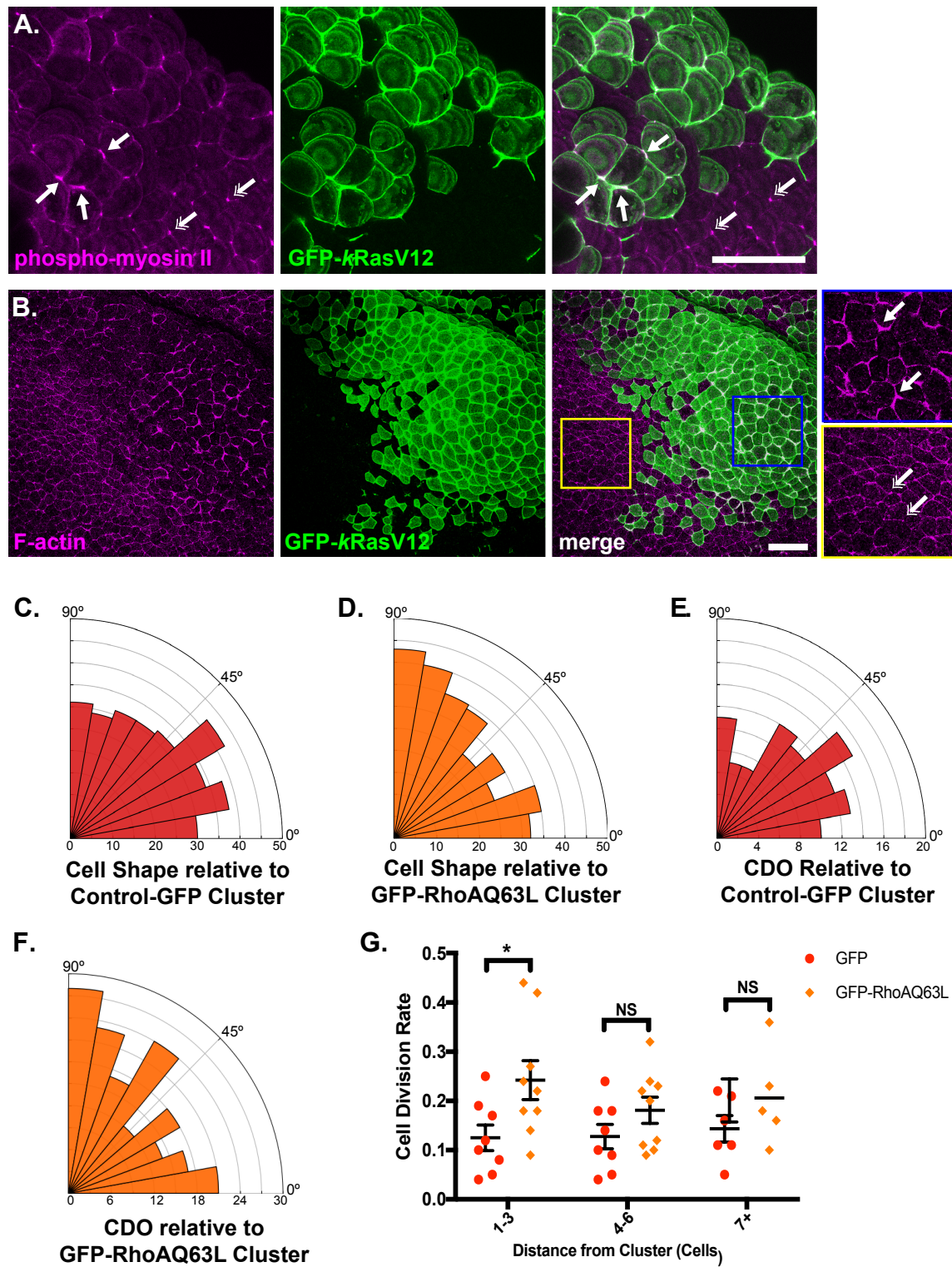


Figure 4: Activation of RhoA in a cell cluster induces a response in the wild-type epithelium comparable to *kRas*^{V12} expression

A. Confocal microscopy image of a fixed, stage 10 embryo with a GFP-*kRas*^{V12} cluster, stained for phosphorylated myosin II (magenta). Single-headed arrows highlight tricellular junctions with increased phosphorylated myosin II in the GFP-*kRas*^{V12} expressing cells compared to wild-type tissue (double-headed arrows). Scale bar is 100 μ m. **B.** Confocal microscopy image of a fixed, stage 10 embryo with a GFP-*kRas*^{V12} cluster, phalloidin-stained for F-actin (magenta). Single-headed arrows highlight increased F-actin at the cell cortex in the GFP-*kRas*^{V12} cluster compared to wild-type tissue (double-headed arrows). Scale bar is 100 μ m. **C-D.** Rose histograms show the orientation of wild-type cells' long-axes up to 6 cells from a (C) GFP-control or (D) GFP-RhoA^{Q63L} cell cluster, relative to the cluster, with the total number of cells that were analysed across all embryos in each data group in 10° bins. Kolmogorov-Smirnov Test: $p=0.0468$, $n=98$ cell from GFP-control embryos and 193 cells from GFP-RhoA^{Q63L} embryos. **E-F.** Rose histograms show cell division orientation relative to (E) GFP-control or (F) GFP-RhoA^{Q63L} clusters, with the total number of cell divisions that were analysed across all embryos in each data group in 10° bins. Kolmogorov-Smirnov Test: $p=0.0368$, $n=310$ divisions from GFP-control embryos and 299 divisions from GFP-RhoA^{Q63L} embryos. **G.** Scatter Plot shows percentage of wild-type cells that divided per minute of time-lapse at different distances from GFP-control or GFP-RhoA^{Q63L} clusters. 1-3 cells: Mann-Whitney U Test: $p=0.0104$, $n=7$ GFP-control, and 9 GFP-RhoA^{Q63L} embryos. 4-6 cells: $p=0.1488$, $n=7$ GFP-control, and 9 GFP-RhoA^{Q63L} embryos. 7+ cells: $p=0.3528$, $n=6$ GFP-control and 5 GFP-RhoA^{Q63L} embryos. Error bars are SEM.

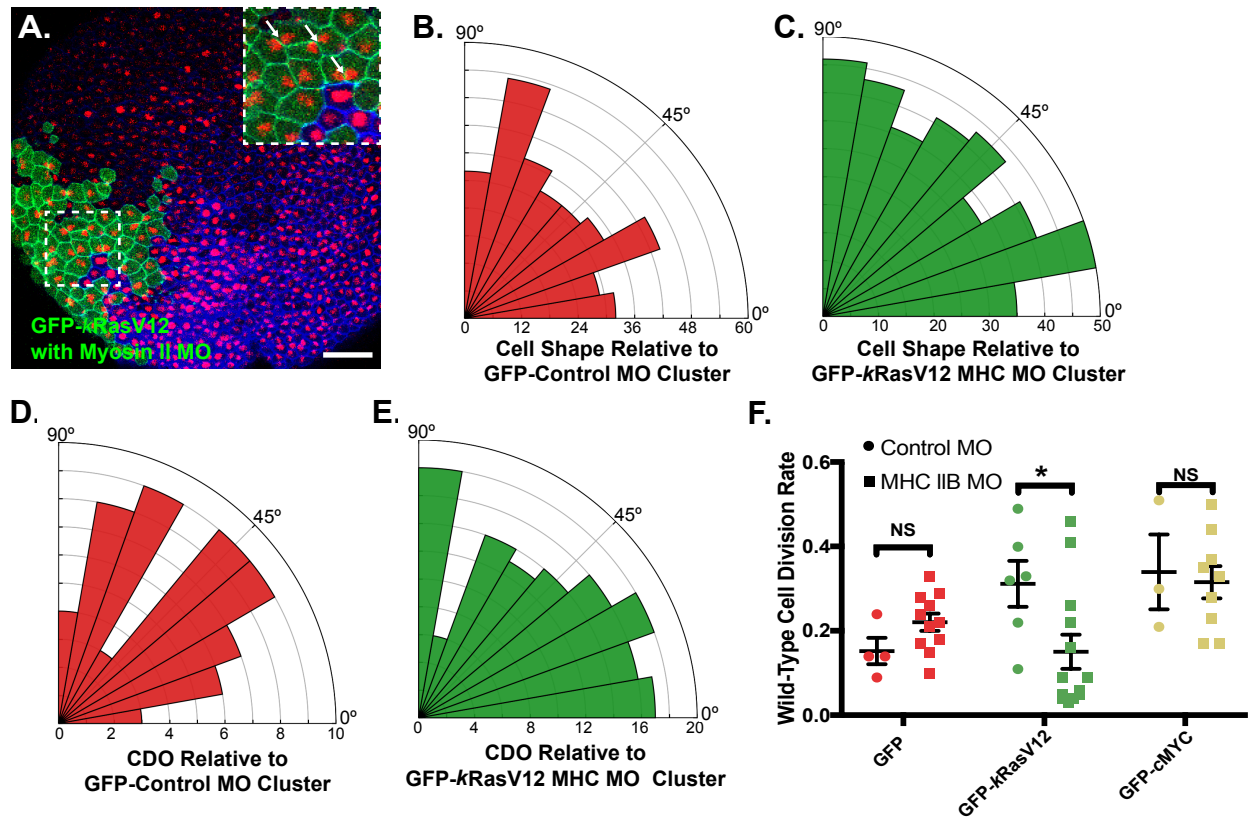


Figure 5: Non-muscle Myosin II is required in *kRas*^{V12}-expressing cells for the cluster to alter wild-type tissue mechanics and cell division

A. Confocal microscopy image shows a myosin II deficient GFP-*kRas*^{V12} cell cluster. Arrows highlight 'butterfly-nuclei'. Scale bar is 100 μ m. **B-C.** Rose histograms show the orientation of wild-type cell long-axes up to 3 cells from (B) GFP control morpholino or (C) myosin II deficient GFP-*kRas*^{V12} cell clusters, with the total number of cells that were analysed across all embryos in each data group in 10° bins. Kolmogorov-Smirnov Test: $p=0.7992$, $n=325$ cells from GFP control MO embryos and 368 cells from GFP-*kRas*^{V12} MHC MO embryos. **D-E.** Rose histograms show cell division orientation up to 6 cells from (D) GFP control morpholino or (E) myosin II deficient GFP-*kRas*^{V12} cell clusters, with the total number of cell divisions that were analysed across all embryos in each data group in 10° bins. Kolmogorov-Smirnov Test: $p=0.4013$, $n=58$ divisions from GFP control MO embryos and 132 divisions from GFP-*kRas*^{V12} MHC MO embryos. **F.** Scatter Plot shows percentage of wild-type cells that divided per minute of time-lapse, up to 3 cells from GFP, GFP-*kRas*^{V12} or GFP-cMYC control morpholino clusters, or myosin II deficient GFP, GFP-*kRas*^{V12} or GFP-cMYC clusters. GFP: Mann-Whitney U Test: $p=0.1211$, $n=5$ GFP control MO embryos and 11 GFP MHC MO embryos, GFP-*kRas*^{V12}: $p=0.0299$, $n=6$ GFP-*kRas*^{V12} control MO embryos and 13 GFP-*kRas*^{V12} MHC MO embryos, GFP-cMYC: $p=0.8318$, $n=3$ GFP-cMYC control MO embryos and 9 GFP-cMYC MHC MO embryos,